

Tunneling spectroscopy for ferromagnet/superconductor junctions

Igor Žutić*

Department of Physics, University of Maryland, College Park, Maryland 20742

Oriol T. Valls†

Department of Physics and Minnesota Supercomputer Institute, University of Minnesota, Minneapolis, Minnesota 55455

(April 6, 2018)

In tunneling spectroscopy studies of ferromagnet/superconductor (F/S) junctions, the effects of spin polarization, Fermi wavevector mismatch (FWM) between the F and S regions, and interfacial resistance play a crucial role. We study the low bias conductance spectrum of these junctions, governed by Andreev reflection at the F/S interface. We consider both d - and s -wave superconductors as well as mixed states of the $d + is$ form. We present results for a range of values of the relevant parameters and find that a rich variety of features appears, depending on pairing state and other conditions. We show that in the presence of FWM, spin polarization can enhance Andreev reflection and give rise to a zero bias conductance peak for an s -wave superconductor.

74.80.Fp, 74.50+r, 74.72-h

I. INTRODUCTION

The development and refinement in recent years of new techniques in materials growth has made it possible to fabricate superconducting heterostructures with various materials and high quality interfaces. These advances, coupled with the continuing intense level of activity in the study of the nature of high temperature¹⁻³ and other exotic superconductors,^{4,5} has led to renewed interest in tunneling spectroscopy.

It has been demonstrated^{3,6,7} that this technique yields information about both the magnitude and the phase of the superconducting pair potential (PP). This implies that the method can provide a systematic way to distinguish among various proposed PP candidates, including both spin singlet and spin triplet pairing states.^{8,9} For example, it has been argued that the observed zero bias conductance peak^{6,7,10-12} (ZBCP), attributed to mid-gap surface states, is an indication of unconventional superconductivity with a sign change of the PP, as it occurs in pairing with a $d_{x^2-y^2}$ -wave symmetry. Furthermore, the splitting of the ZBCP and the forming of a finite bias peak (FBCP) in the conductance spectrum has been examined and interpreted¹³⁻¹⁵ as support for the admixture of an imaginary PP component to the dominant $d_{x^2-y^2}$ -wave part, leading to a broken time-reversal symmetry.^{16,17}

The same developments, and the ability to make low interfacial resistance junctions between high spin polarization ferromagnets and superconductors, have stimulated significant efforts to study transport in these structures.¹⁸ There have been various experiments in both conventional¹⁹⁻²¹ and high temperature superconductors²²⁻²⁵ (HTSC's), as well as re-examinations of earlier work^{26,27} which was performed generally in the tunneling limit of strong interfacial barrier. Theoretical studies of the effects of spin polarized transport on the current-voltage characteristics and the conductance in ferromagnet/superconductor (F/S) junctions have been carried out in conventional²⁸ and, recently, in high-temperature superconductors.²⁹⁻³¹ The feasibility of nanofabricating F/S structures has also generated interest in studying the influence of ferromagnetism on mesoscopic superconductivity.³²

One of the important questions raised by the possibility of making high transmissivity F/S junctions was that of studying the influence of Andreev reflection (AR)^{28,33-35} on spin polarized transport. In AR an electron, belonging to one of the two spin bands, incoming from the ferromagnetic region to the F/S interface will be reflected as a hole in the opposite spin band. The splitting of spin bands by the exchange energy in ferromagnetic materials implies that only a fraction of the incoming incident majority spin electrons can be Andreev reflected.²⁸ This simple argument was used in previous studies^{19,20,28} to infer that the effect of spin polarization (exchange energy) was generally to reduce AR. The sensitivity of AR to the exchange energy in a ferromagnet was employed^{19,20} to determine the degree of polarization in various materials.

In this paper we will study the tunneling spectroscopy of F/S junctions. We will adopt the basic approach of Ref. 36 but we will extend and generalize it to include the effects of spin polarization, the presence of an unconventional PP state (pure or mixed), and the existence of Fermi wavevector mismatch (FWM)^{37,38} stemming from the different band widths in the two junction materials. Our aim in this paper is twofold: Firstly, to investigate and reveal novel features in the conductance spectra arising from the interplay of ferromagnetism and unconventional superconductivity, and secondly, to show the importance of FWM, and how its inclusion can lead to some unexpected results, even for F/s-

wave superconductor junctions, where we find, for example, that in some cases Andreev reflection can be enhanced by spin polarization.

In the next section (Sec. II), we present the methods we use to obtain the amplitudes for the various scattering processes that occur in the junction when spin polarized electrons are injected from the F into the S region. We will use these methods to calculate the conductance of the F/S junctions. In Sec. III, we first give results for a conventional (*s*-wave) superconductor in the S side, and then illustrate the unconventional case of the pairing potential by considering both pure *d*- and mixed *d* + *is*-wave symmetry. In Sec. IV, we summarize our results and discuss future problems.

II. METHODS

As explained in the Introduction, we investigate in this work F/S junctions by extending and generalizing the techniques previously employed in the study of simpler cases without spin polarization, or for conventional superconductors. Thus, we use here the Bogoliubov-de Gennes (BdG) equations^{6,7,28,34,39} in the ballistic limit. We consider a geometry where the ferromagnetic material is at $x < 0$, and is described by the Stoner model. We take the usual approach²⁸ of assuming a single particle Hamiltonian with the exchange energy being therefore of the form $h(\mathbf{r}) = h_0\Theta(-x)$, where $\Theta(x)$ is a step function. The F/S interface is at $x = 0$, where there is interfacial scattering modeled by a potential $V(\mathbf{r}) = H\delta(x)$,^{7,19,20,36} and H is the variable strength of the potential barrier. The dimensionless parameter characterizing barrier strength³⁶ is $Z_0 \equiv mH/\hbar k_F$, where the effective mass, m , is taken to be equal in the F and S regions. In the superconducting region, at $x > 0$, we assume^{6,7,28,36,40} that there is a pair potential $\Delta(\mathbf{k}', \mathbf{r}) = \Delta(\mathbf{k}')\Theta(x)$. This approximation for the PP becomes more accurate⁴¹ in the presence of FWM and allows analytic solution of the BdG equations. We will denote quantities pertaining to the S region by primed letters.

From these considerations, the BdG equations for F/S junction, in the absence spin-flip scattering, can be written as³⁹

$$\begin{bmatrix} H_0 - \rho_S h & \Delta \\ \Delta^* & -(H_0 + \rho_S h) \end{bmatrix} \begin{bmatrix} u_S \\ v_{\bar{S}} \end{bmatrix} = \epsilon \begin{bmatrix} u_S \\ v_{\bar{S}} \end{bmatrix}, \quad (2.1)$$

where H_0 is the single particle Hamiltonian and $\rho_S = \pm 1$ for spin $S = \uparrow, \downarrow$. The exchange energy $h(\mathbf{r})$ and the PP Δ are as defined above. The excitation energy is denoted by ϵ , and u_S , $v_{\bar{S}}$ are the electronlike quasiparticle (ELQ) and holelike quasiparticle (HLQ) amplitudes, respectively. We take $H_0 \equiv -\hbar^2 \nabla^2 / 2m + V(\mathbf{r}) - E_F^{F,S}$, where $V(\mathbf{r})$ is defined above. In the F region, we have $E_F^F \equiv E_F = \hbar^2 k_F^2 / 2m$, so that E_F is the spin averaged value, $E_F = (\hbar^2 k_{F\uparrow}^2 / 2m + \hbar^2 k_{F\downarrow}^2 / 2m) / 2$. We assume that in general it differs from the value in the superconductor, $E_F^S \equiv E_F' = \hbar^2 k_F'^2 / 2m$. Thus, we take the Fermi energies to be different in the F and S regions that is, we allow for different band widths, stemming from the different carrier densities in the two regions. Indeed, as the results in the next Section will show, the Fermi wavevector mismatch (FWM) between the two regions has an important influence on our findings. We will parameterize the FWM by the value of L_0 , $L_0 \equiv k_F' / k_F$ and describe the degree of spin polarization, related to the exchange energy, by the dimensionless parameter $X \equiv h_0 / E_F$.

The invariance of the Hamiltonian with respect to translations parallel to $x = 0$ implies conservation⁴² of the (spin dependent) parallel component of the the wavevector at the junction. As we shall show, this will be an important consideration in understanding the possible scattering processes. An electron injected from the F side, with spin $S = \uparrow, \downarrow$, excitation energy ϵ , and wavevector \mathbf{k}_S^+ (with magnitude $k_S^+ = (2m/\hbar^2)^{1/2}[E_F + \epsilon + \rho_S h_0]^{1/2}$), at an angle θ from the interface normal, can undergo four scattering processes^{7,36} each described by a different amplitude. Assuming specular reflection at the interface, these can be characterized as follows: 1) Andreev reflection, with amplitude that we denote by a_S , as a hole with spin, \bar{S} , belonging to the spin band opposite to that of the incident electron ($\rho_{\bar{S}} = -\rho_S$), wavevector $\mathbf{k}_{\bar{S}}^-$ ($k_{\bar{S}}^- = (2m/\hbar^2)^{1/2}[E_F - \epsilon + \rho_{\bar{S}} h_0]^{1/2}$), and spin dependent angle of reflection $\theta_{\bar{S}}$, generally different from θ .³⁰ As is the case with the angles corresponding to the other scattering processes, $\theta_{\bar{S}}$, as we shall see below, is determined from the requirement that the parallel component of the wavevector is conserved. Even in the absence of exchange energy ($h_0 = 0$), one has that, for $\epsilon \neq 0$, $\theta_{\bar{S}}$ (although then spin independent) is slightly different⁴³ from θ . When $h_0 > 0$, the typical situation is, as we discuss later, that $|\theta_{\downarrow}| < |\theta| < |\theta_{\uparrow}|$. 2) The second process is ordinary reflection into the F region, characterized by an amplitude which we call b_S , as an electron with variables S , $-\mathbf{k}_S^+$, $-\theta$. The other two processes are: 3) Transmission into the S region, with amplitude c_S , as an ELQ with \mathbf{k}_S^+ , and 4) Transmission as a HLQ with amplitude d_S and wavevector $-\mathbf{k}_{\bar{S}}^-$. Here the corresponding wavevector magnitudes are $k_S^{\pm} = (2m/\hbar^2)^{1/2}[E_F' \pm (\epsilon^2 - |\Delta_{S\pm}|^2)^{1/2}]^{1/2}$. We denote by $\Delta_{S\pm} = |\Delta_{S\pm}| \exp(i\phi_{S\pm})$, the different PP's felt by the ELQ and the HLQ, respectively, as determined by \mathbf{k}_S^{\pm} . We see, therefore, that up to four different energy scales of the PP are involved for each incident angle θ . In our considerations, which pertain to the common experimental situation,^{44,45} $E_F, E_F' \gg \max(\epsilon, |\Delta_{S\pm}|)$, we can employ the Andreev approximation^{7,28,33,34}

and write $k_S^\pm \approx k_{FS} \equiv (2m/\hbar^2)^{1/2}[E_F + \rho_S \hbar_0]^{1/2}$, $k_S'^\pm \approx k_F'$. It then follows that the appropriate wavevectors for the transmission of ELQ's and HLQ's are at angles θ'_S , $-\theta'_S$, with the interface normal, respectively. Within this approximation the components of the vectors \mathbf{k}_S^\pm , $\mathbf{k}_S'^\pm$ normal and parallel to the interface, can be expressed as $\mathbf{k}_S^\pm \equiv (k_S, k_{\parallel S})$, and $\mathbf{k}_S'^\pm \equiv (k'_S, k_{\parallel S})$, in the F and S regions. From the conservation of $k_{\parallel S}$, we have then an analogue of Snell's law

$$k_{FS} \sin \theta = k_{F\bar{S}} \sin \theta_{\bar{S}}, \quad (2.2a)$$

$$k_{FS} \sin \theta = k'_F \sin \theta'_S, \quad (2.2b)$$

which has several important implications, including the existence of critical angles,⁴⁶ as one encounters in well known phenomena in the propagation of electromagnetic waves.⁴⁷

Using the conservation of $k_{\parallel S}$, the solution to Eq. (2.1), $\Psi_S \equiv (u_S, v_S)^T$, can be expressed in a separable form, effectively reducing the problem to a one-dimensional one. In the F region we write

$$\Psi_S(\mathbf{r}) \equiv e^{i\mathbf{k}_{\parallel S} \cdot \mathbf{r}} \psi_S(x), \quad (2.3)$$

where

$$\psi_S(x) = e^{ik_S x} \begin{bmatrix} 1 \\ 0 \end{bmatrix} + a_S e^{ik_{\bar{S}} x} \begin{bmatrix} 0 \\ 1 \end{bmatrix} + b_S e^{-ik_S x} \begin{bmatrix} 1 \\ 0 \end{bmatrix}, \quad (2.4)$$

analogously, in the S region we have⁷

$$\Psi'_S(\mathbf{r}) \equiv e^{i\mathbf{k}_{\parallel S} \cdot \mathbf{r}} \psi'_S(x), \quad (2.5)$$

$$\psi'_S(x) = c_S e^{ik'_S x} \begin{bmatrix} (\epsilon + \Omega_{S+}/2\epsilon)^{\frac{1}{2}} \\ e^{-i\phi_+} (\epsilon - \Omega_{S+}/2\epsilon)^{\frac{1}{2}} \end{bmatrix} + d_S e^{-ik'_S x} \begin{bmatrix} e^{i\phi_-} (\epsilon - \Omega_{S-}/2\epsilon)^{\frac{1}{2}} \\ (\epsilon + \Omega_{S-}/2\epsilon)^{\frac{1}{2}} \end{bmatrix}, \quad (2.6)$$

with $\Omega_{S\pm} \equiv (\epsilon^2 - |\Delta_{S\pm}|^2)^{\frac{1}{2}}$, and the appropriate boundary conditions^{7,36} at the F/S interface are

$$\psi_S(0) = \psi'_S(0), \quad \partial_x \psi_S(0) - \partial_x \psi'_S(0) = \frac{2mH}{\hbar^2} \psi'_S(0). \quad (2.7)$$

We pause next to discuss some implications of Eq. (2.2) for the various scattering processes. In typical realizations of ferromagnet/HTSC structures, the appropriate FWM corresponds to $L_0 \leq 1$.⁴⁴ Consider first $L_0 = 1$, i.e. $E_F = E'_F$. If $X > 0$ it follows that $k_{F\downarrow} < k'_F < k_{F\uparrow}$, for an $S = \downarrow$ incoming electron. Then, at any incident angle, Eq. (2.2) is satisfied so that k_{\parallel} will be conserved. In this case $|\theta| > |\theta'_\downarrow| > |\theta'_\uparrow|$, and all the corresponding wave vectors are real. For an $S = \uparrow$ incident electron at angle $|\theta| > |\sin^{-1}(k'_F/k_{F\uparrow})|$, a solution of Eq. (2.2b) for a real θ'_\uparrow no longer exist, one has a complex θ'_\uparrow .⁴⁷ The scattering problem does not have a solution with propagating wavevectors in the S region: there is total reflection. The wavevectors for ELQ and HLQ have purely imaginary components along the x -axis, while their components parallel to the interface are real. This corresponds to a surface (evanescent) wave, propagating along the interface and exponentially damped away from it.⁴⁷ An analogous, but physically more interesting, situation occurs for AR in the particular case where $|\theta|$ is smaller than the angle of total reflection and satisfies $|\theta| > |\sin^{-1}(k_{F\downarrow}/k_{F\uparrow})|$. This regime corresponds to $k_{\parallel\uparrow} > k_{F\downarrow}$. In this case it is Eq. (2.2a) that has no solution for real angles. This means that Andreev reflection as a *propagating* wave is impossible. From the condition, which follows from the Andreev approximation, $k_{\uparrow}^2 + k_{\parallel\uparrow}^2 \equiv k_{F\downarrow}^2$, we see that the component k_{\uparrow} along the x axis must be purely imaginary,³¹ while $k_{\parallel\uparrow}$ is still real. With these considerations we then find

$$k_{\uparrow} = -i(k_{F\uparrow}^2 \sin^2 \theta - k_{F\downarrow}^2)^{1/2}, \quad (2.8)$$

where we have expressed k_{\uparrow} in terms of quantities which are always real and which pertain to the F region only. As with total reflection, there is propagation only along the interface and an exponential decay away from it. This case differs from that of total reflection in that, since the evanescence affects only the Andreev reflected component, there may still be transmission across the junction.

The above considerations apply *a fortiori* in the presence of FWM. For example, if we now consider $L_0 < 1$, we can see by inspection of Eq. (2.2), that there can also be total reflection for an $S = \downarrow$ incident electron, when $k_{F\downarrow} > k'_F$. This condition would imply the absence of imaginary k_{\uparrow} for any incident angle and any exchange energy.

Returning now to the basic equations, we see that by solving for $\psi_S(x)$, $\psi'_S(x)$ in Eq. (2.4), (2.6) with the boundary conditions given by Eq. (2.7), we can obtain the amplitudes a_S , b_S , c_S and d_S , $S = \uparrow, \downarrow$. For each spin, there is a sum rule, related to the conservation of probability, for the squares of the absolute values of the amplitudes. We can thus, in a way similar to what was done in Ref. 36, express the various quantities in terms of the amplitudes a_S and b_S only. These amplitudes are given by

$$a_S = \frac{4t_S L_S \Gamma_+ e^{-i\phi_{S+}}}{U_{SS+} U_{\bar{S}S-} - V_{SS-} V_{\bar{S}S+} \Gamma_+ \Gamma_- e^{i(\phi_{S-} - \phi_{S+})}}, \quad (2.9)$$

$$b_S = \frac{V_{SS+} U_{\bar{S}S-} - U_{SS-} V_{\bar{S}S+} \Gamma_+ \Gamma_- e^{i(\phi_{S-} - \phi_{S+})}}{U_{SS+} U_{\bar{S}S-} - V_{SS-} V_{\bar{S}S+} \Gamma_+ \Gamma_- e^{i(\phi_{S-} - \phi_{S+})}}, \quad (2.10)$$

where we have introduced the notation $\Gamma_{\pm} \equiv (\epsilon - \Omega_{S\pm})/|\Delta_{S\pm}|$, $L_S \equiv L_0 \cos \theta'_S / \cos \theta$, describing FWM, $t_S \equiv k_S/k_{Fx} = (1 + \rho_S X)^{1/2}$, $t_{\bar{S}} \equiv k_{\bar{S}}/k_{Fx} = (1 - \rho_S X)^{1/2} \cos \theta_{\bar{S}} / \cos \theta$, for $k_{\bar{S}}$ real, $(-i[(1+X)\sin^2 \theta - (1-X)]^{1/2} / \cos \theta$, for $k_{\bar{S}}$ imaginary, see Eq. (2.8)). The other abbreviations are defined as: $U_{\bar{S}S\pm} \equiv t_{\bar{S}} + w_{S\pm}$, $V_{SS\pm} \equiv t_S - w_{S\pm}$, $w_{S\pm} \equiv L_S \pm 2iZ$, $Z \equiv Z_0 / \cos \theta$, where $Z_0 \equiv mH/\hbar k_F$ is the interfacial barrier parameter, as defined above. The limits $Z_0 \rightarrow 0$ and $Z_0 \rightarrow \infty$ correspond to the extreme cases of a metallic point contact and the tunnel junction limit, respectively.

Given the above amplitudes, the results for the dimensionless differential conductance³⁶ can be written down in the standard way by computing, as a function of the excitation energy arising from the application of a bias voltage, the ratio of the induced flux densities across the junction to the corresponding incident flux density. One straightforwardly generalizes the methods used in previous work^{7,36,48} to include now the effects of unconventional superconductivity, FWM, and net spin polarization, to obtain,

$$G \equiv G_{\uparrow} + G_{\downarrow} = \sum_{S=\uparrow, \downarrow} P_S \left(1 + \frac{k_{\bar{S}}}{k_S} |a_S|^2 - |b_S|^2\right), \quad (2.11)$$

where we introduce the probability P_S of an incident electron having spin S , related to the exchange energy as $P_S = (1 + \rho_S X)/2$.²⁸ In deriving Eq. (2.11), care has to be taken to properly include the flux factors, which are, at $X > 0$, different for the incident and the Andreev reflected particle. The ratio of wavevectors in the second term on the right side of Eq. (2.11) results from the incident electron and the AR hole belonging to different spin bands. The quantity $k_{\bar{S}}$ in that term is real, the case of imaginary $k_{\bar{S}}$ can only contribute to G_{\uparrow} indirectly, by modifying $|b_{\uparrow}|$. It can be shown³⁰ from the conservation of probability current³⁶ that such a contribution vanishes for the subgap conductance ($\epsilon < |\Delta_{\uparrow\pm}|$).⁴⁹ It is, furthermore, possible to express the subgap conductance in terms of the AR amplitude only.³⁰ At $X = 0$ we recover the results of Ref. 7. The suppression of the conductance due to ordinary reflection at $X \neq 0$ has the same form as for the unpolarized case since the magnitude of the normal component of the wavevectors before and after ordinary reflection remains the same.

We focus in this work (see results in the next Section) on the conductance spectrum of the charge current as given by Eq. (2.11), but the amplitudes a_S , b_S , given by Eq. (2.9), (2.10) can be used to calculate many other quantities of interest, such as current-voltage characteristics, the spin current, and the spin conductance.³¹ We consider also here angularly averaged quantities and notice that Eq. (2.11) implies that the conductance vanishes for $|\theta|$ greater than the angle of total reflection (we recall that this angle is spin dependent). We define the angularly averaged (AA) conductance, $\langle G_S \rangle$, as

$$\langle G_S \rangle = \int_{\Omega_S} d\theta \cos \theta G_S(\theta) / \int_{\Omega_S} d\theta \cos \theta, \quad (2.12)$$

where Ω_S is limited by the angle of total reflection or by experimental setup. This form correctly reduces to that used in the previously investigated spin unpolarized situation.⁷ One may choose a different weight function in performing such angular averages, depending on the specific experimental geometry and the strengths of the interfacial scattering.^{11,48,50} However, all expressions for angularly averaged results, obtained from different averaging methods, would still have a factor of $(1 + \frac{k_{\bar{S}}}{k_S} |a_S|^2 - |b_S|^2)$ in the kernel of integration, and would merely require numerical integration of the amplitudes we have already given here.

III. RESULTS

A. Conventional pair potentials

We present our results in terms of the dimensionless differential conductance, plotted as a function of the dimensionless energy $E \equiv \epsilon/\Delta_0$. We concentrate on the region $E \lesssim 1$ since for larger bias various extrinsic effects, such as heating, tend to dominate the behavior of the measured conductance.⁵¹ While our findings, and the analytic results from Section II, are valid for any value of the interfacial scattering, we focus on smaller values of Z_0 , $Z_0 \leq 1$, where the novel effects of ferromagnetism on Andreev reflection, and consequently on the conductance, are more pronounced than in the tunneling limit, $Z_0 \gg 1$. This regime on which we focus is also that which is believed to correspond to several ongoing experiments of F/S structures, where the samples typically have small interface resistance.^{24,25} To present numerical results, we choose $E_F/\Delta_0 = 12.5$, consistent with optimally doped $YBa_2Cu_3O_{7-\delta}$.^{52,53} We will include FWM, as parametrized by the quantity L_0 introduced above, $E_F = E'_F/L_0^2$.

We first give some results for an s -wave PP, with a constant energy gap. This will serve to illustrate the influence of FWM coupled with that of Z_0 within a simpler and more familiar context. In this case, for any incident angle, θ , of an injected electron the ELQ and HLQ feel the same PP with $\Delta_{S\pm} = \Delta_0$, and $\phi_{S\pm} \equiv 0$. Therefore, the results that we give here for the s -wave case and normal incidence ($\theta = 0$), also correspond to the case of a PP of the $d_{x^2-y^2}$ form, with the angle $\alpha \in (-\pi/2, \pi/2)$, between the crystallographic a -axis and the interface normal, set to $\alpha = 0$. This would represent an F/S interface along the (100) plane.

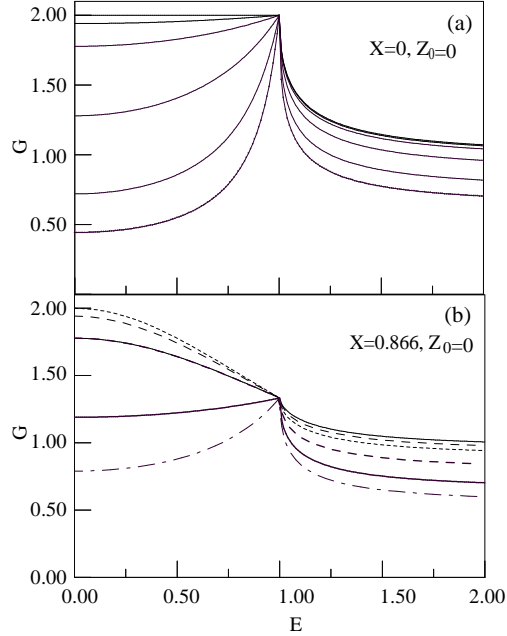


FIG. 1. $G(E)$ (Eq.(2.11)) versus $E \equiv \epsilon/\Delta_0$. Results are for $\theta = 0$ (normal incidence). The curves are for $Z_0 = 0$ (no barrier): in panel (a) at exchange energy $X \equiv h_0/E_F = 0$ (no spin polarization) they are (from top to bottom at any E) for the FWM values of $L_0^2 = E'_F/E_F = 1, 1/\sqrt{2}, 1/2, 1/4, 1/9, 1/16$. In panel (b) they are for $X = 0.866$. Since the curves now cross at $E = 1$ they are drawn in different ways for clarity. For $E > 1$ they are in the same order as in panel (a) and for the same values of L_0 , while for $E < 1$ they correspond, from top to bottom, to $L_0^2 = 1/2, 1/\sqrt{2}, 1, 1/9, 1/16$. The $L_0^2 = 1/4$ curve overlaps with that for $L_0^2 = 1$ in this range.

In Fig. 1 we show results for $G(E)$, given by Eq. (2.11), at $\theta = 0$, and $Z_0 = 0$ (this limit of no interfacial barrier was also considered in Ref. 28). We plot results for various values of the FWM parameter L_0 . Panel (a) corresponds to no polarization ($X = 0$) and panel (b) to high polarization $X = \sqrt{3}/2 \approx 0.866$. For normal incidence, we have $t_S = (1 + \rho_S X)^{1/2}$, $t_{\bar{S}} = (1 - \rho_S X)^{1/2}$ (as defined below Eq. (2.10)), and the subgap conductance can be expressed as

$$G = \frac{32L_0^2(1 - X^2)^{1/2}}{|t_{\uparrow}t_{\downarrow} + (t_{\uparrow} + t_{\downarrow})L_0 + L_0^2 - (t_{\uparrow}t_{\downarrow} - (t_{\uparrow} + t_{\downarrow})L_0 + L_0^2)\Gamma_+\Gamma_-|^2}. \quad (3.1)$$

Panel (a) displays results in the absence of exchange energy. With increasing FWM (i.e. decreasing L_0), the amplitude at zero bias voltage (AZB) decreases monotonically. This effect was explained³⁷ in previous work as resulting from the increase in a single parameter Z_{eff} , which combined Z_0 with the effects of FWM. Our curves with FWM ($L_0 < 1$)

reduce in the appropriate limits to those previously found³⁷ with $L_0 = 1$ and $Z_0 \rightarrow Z_{eff}$, $Z_{eff} > Z_0$. We will see below that this is not the case at $X \neq 0$. In panel (b) we give results for high X while keeping the other parameters at the same values as in panel (a). We notice that the presence of exchange energy gives rise to non-monotonic behavior in the AZB. At low bias, the conductance can be enhanced with increasing FWM (compare, for example, the $L_0 = 1$ and $L_0 = 1/\sqrt{2}$ results), and form a zero bias conductance peak (ZBCP.) This behavior is qualitatively different from that found in the unpolarized case and the effect of FWM can no longer be reproduced by simply increasing the interface scattering parameter. Thus the often implied^{19,20} expectation that the effects of Z_0 and L_0 could also be subsumed in a single parameter in the spin polarized case is not fulfilled. In this panel we have an example of coinciding subgap conductances for $L_0 = 1$ and $L_0 = 1/2$. The condition for this coincidence to take place at fixed X can be simply obtained from Eq. (3.1) as

$$t_{\uparrow}t_{\downarrow}/L_0^2 = L_0'^2 \Rightarrow (1 - X^2) = L_0'^2 (L_0 \equiv 1), \quad (3.2)$$

where L_0, L_0' correspond to two different values of FWM for which the subgap conductances will coincide.

We next look, in the same situation as in the previous figure, at the effects of the presence of an interfacial barrier.

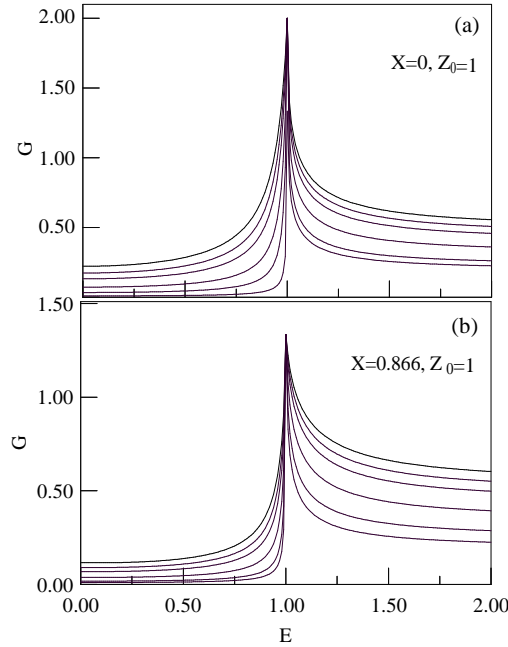


FIG. 2. $G(E)$ for $\theta = 0$ and interfacial barrier strength $Z_0 = 1$. All the other parameters are taken as in the previous figure. In both panels, curves from top to bottom correspond to decreasing values of L_0 .

In Fig. 2, we choose $Z_0 = 1$, while keeping all the other parameters the same as in the corresponding panel of the previous figure. In panel (a) we show results in the absence of spin polarization. A finite bias conductance peak (FBCP) appears at the gap edge. It becomes increasingly narrow with greater FWM (smaller L_0). Its amplitude is 2, independent of L_0 . In panel (b), at $X = 0.866$, the conductance curves display similar behavior, but with a reduced FBCP at the gap edge. From Eqs. (2.9), (2.10), and (2.11), the amplitude of the FBCP in this case is

$$G(E = 1) = \frac{4(1 - X^2)^{1/2}}{1 + (1 - X^2)^{1/2}}. \quad (3.3)$$

An interesting feature of this result is that it depends only on the exchange energy (spin polarization) and not on the FWM parameter or the barrier strength. It can be shown that this property holds for all angles of incidence. This is in contrast with the value of the zero bias conductance which depends, both for normal incidence and for other angles, on the value of the FWM. This dependence could introduce difficulties in the accurate determination of spin polarization from the AZB.^{19,20} The gap edge value is less susceptible to these problems.

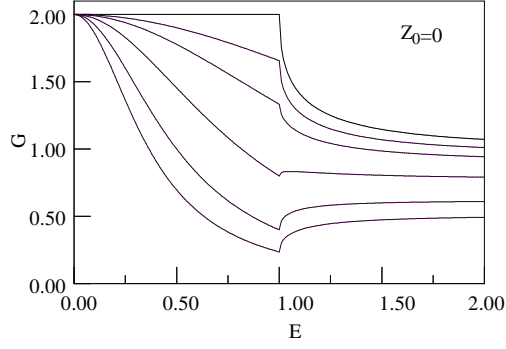


FIG. 3. Evolution of the zero bias conductance, $G(E)$ for $\theta = 0$. Results are given at $Z_0 = 1$ for X determined from Eq. (3.4) and values of L_0 as in Fig. 1. From top to bottom the curves correspond to values of (L_0^2, X) given by $(1, 0)$, $(1/\sqrt{2}, 1/\sqrt{2})$, $(1/2, 0.866)$, $(1/4, 0.968)$, $(1/9, 0.994)$, and $(1/16, 0.998)$.

The presence of spin polarized carriers, due to nonvanishing exchange energy, is usually held^{20,28,29} to result in the suppression of Andreev reflection and thus in a reduction of the subgap conductance. A simple explanation,²⁸ which neglects the effects of FWM, predicts that the AZB should monotonically decrease with increasing X , because of the reduction of Andreev reflection, when only a fraction of injected electrons from the majority spin band can be reflected as holes belonging to the minority spin band. This follows from the reduction of the density of states in the minority spin band with increasing X , and eventually causes the subgap conductance to vanish for a half-metallic ferromagnet when $X \rightarrow 1$.

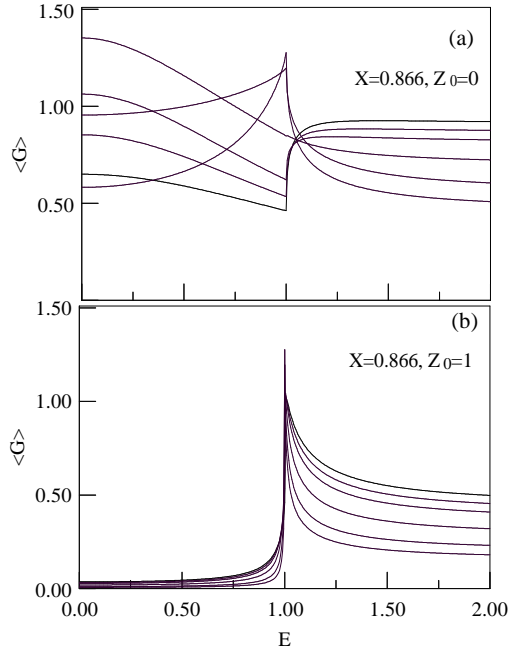


FIG. 4. $\langle G(E) \rangle$, the θ averaged conductance, for an s -wave PP and the same values of X , L_0 as in panels (b) of Figs. 1, 2, respectively. In both panels curves from top to bottom, at $E = 2$, correspond to decreasing L_0 .

We now proceed to examine whether these findings are modified when FWM is taken into account. In Fig. 3, which shows results at $Z_0 = 0$ and normal incidence, we consider the evolution of the conductance curves for different values of X and L_0 chosen to yield maximum AZB, ($G(E = 0) = 2$), starting from the step-like feature at $L_0 = 1$ and $X = 0$ (see Fig. (1)). The condition for maximum AZB at fixed FWM and polarization can be derived³⁰ from Eq. (3.1) and is

$$k_{\uparrow}k_{\downarrow} = k_F^2 \Rightarrow (1 - X^2)^{1/2} = L_0^2. \quad (3.4)$$

We have used this equation to determine the optimal value of X for each value of L_0 used in Figs. 1, 2. The

resulting curves are plotted in Fig. 3. This figure reveals several interesting features. With the increase of FWM and the correspondingly larger optimal spin polarization (according to the value of X found from Eq. (3.4)), a ZBCP forms. This is a novel effect in which the peak arises from a mechanism completely different from the one usually put forward, where the ZBCP is attributed to the presence of unconventional superconductivity. In that case, the ZBCP is produced by the sign change of the PP and the concomitant formation of Andreev bound states.^{6,7,12} Furthermore, if we compare these curves with those in panel (b) of Fig. 1, we see that the subgap conductance can increase with increasing spin polarization at fixed L_0 . This implies that Andreev reflection can be enhanced by spin polarization.

We now turn to angular averages (AA). In Fig. 4 we show angularly averaged results, obtained from the expression for $\langle G \rangle$, Eq. (2.12). The averaged results are no longer equivalent (as in the previous figures with normal incidence) to the case of a $d_{x^2-y^2}$ PP with an F/S interface along the (100) plane: the angular dependence of the PP would then modify the results. Each of the two panels shown includes results for the same set of parameter values used in panels (b) of Figs. 1, and 2, respectively. In panel (a) of the current figure we show how the novel features previously discussed are largely preserved after angular averaging. There is still formation of a ZBCP with increased FWM and the AZB retains its non-monotonic behavior with L_0 , as in the case of fixed normal incidence. The angularly averaged results in panel (b), at $Z_0 = 1$, display behavior similar to that found in the $\theta = 0$ case, with the conductance peak at $E = 1$ becoming sharper at increasing FWM.

B. Unconventional pair potentials

We next consider an angularly dependent PP, specifically that for a $d_{x^2-y^2}$ pairing state. With this PP we have different, spin dependent, PP's for ELQ's and HLQ's. These are given respectively by $\Delta_{S\pm} = \Delta_0 \cos(2\theta'_{S\pm})$, where $\theta'_{S\pm}$ can be expressed as $\theta'_{S\pm} = \theta'_S \mp \alpha$ (we recall that α is the angle between the interface normal and the crystallographic a -axis, and θ'_S is related to θ through Eq. (2.2)).

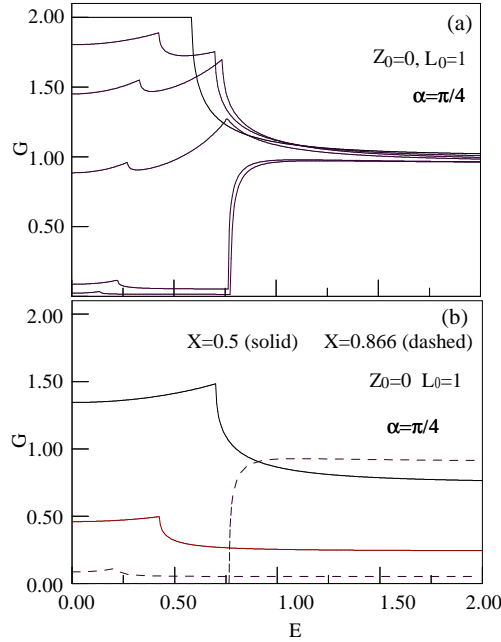


FIG. 5. $G(E)$ for $\theta = \pi/10$, $\alpha = \pi/4$, $Z_0 = 0$, and $L_0 = 1$. In (a) the curves are for $X = 0, 0.5, 0.7, 0.8, 0.866, 0.95$, (top to bottom at $E = 0$). In (b), we plot the spin resolved conductance, for two values of X . The upper curve at $E > 1$ corresponds to G_+ , and the lower curve to G_- .

In Fig. 5 we give some of our results for d -wave pairing and $\alpha = \pi/4$ (interface in the (110) plane), in the absence of both interfacial barrier and FWM and at a fixed $\theta = \pi/10$, for various values of X . Panel (a) shows curves for the total conductance as it evolves from a step-like feature at $X = 0$ to a zero bias conductance dip (ZBCD) for large spin polarization. The width of the plateau at $X = 0$ is determined by a single energy scale set by the equal magnitudes of the PP's for ELQ and HLQ in that case, as given by $\Delta_{S+} = \Delta_{S-} < \Delta_0$, $S = \uparrow, \downarrow$. As the exchange energy is increased, $k_{F\uparrow}$ and $k_{F\downarrow}$ are no longer equal. As one can see from Eq. (2.2b), it follows that $\theta'_\uparrow \neq \theta'_\downarrow$ and

thus $\Delta_{\uparrow\pm} \neq \Delta_{\downarrow\pm}$. These two different energy scales are responsible for the position of various features, such as the several finite bias conductance peaks (FBCP's) that are seen.

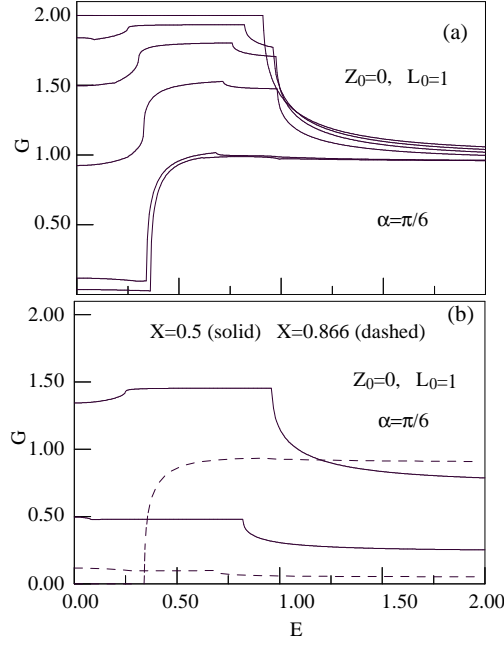


FIG. 6. $G(E)$ for $\theta = \pi/10$, $\alpha = \pi/6$, $Z_0 = 0$, and $L_0 = 1$. In both panels ordering and values of X for each curve are as in Fig. 5.

In panel (b) we show the spin decomposition $G = G_{\uparrow} + G_{\downarrow}$, which better reveals these scales, at two different exchange energies. At $X = 0.5$, the shapes of G_{\uparrow} , G_{\downarrow} are only slightly modified from those in the unpolarized case.

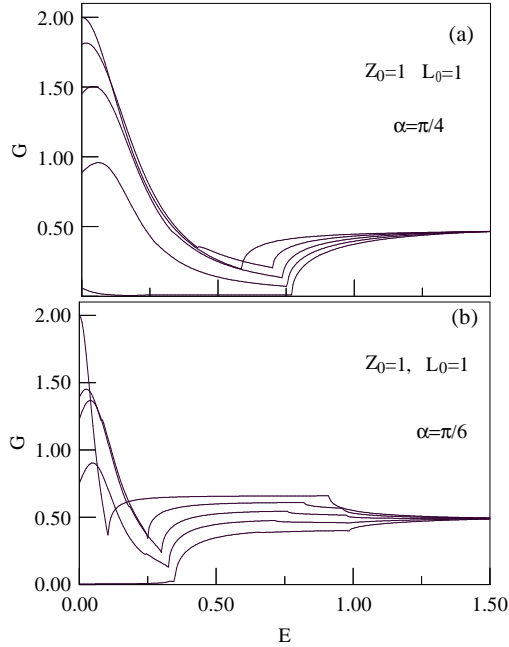


FIG. 7. $G(E)$ for $\theta = \pi/10$, $Z_0 = 1$, and $L_0 = 1$. In both panels curves (top to bottom at $E = 0$) correspond to $X = 0, 0.5, 0.7, 0.8, 0.9$. In (a) $\alpha = \pi/4$, and in (b) $\alpha = \pi/6$.

At larger exchange energy, $X = 0.866$, the situation is very different, as shown in the figure. We also see, in panel

(b), that as stated in the previous section, the evanescent wave associated with the imaginary k_{\uparrow} does not contribute to the subgap conductance G_{\uparrow} .

In general, for an arbitrary orientation of the F/S interface, $\alpha \neq 0, \pi/4$, at a fixed θ , all the four spin dependent PP's for ELQ and HLQ will have different magnitudes. There are, therefore, specific features at four different energy scales. It is only for the particular and atypical (but often chosen in theoretical work) case of $\alpha = \pi/4$ that these four scales reduce to two.

In Fig. 6 we show the general behavior by choosing $\alpha = \pi/6$, while retaining the values of all the other parameters from the previous figure. One can easily calculate, for example, that at $X = 0.5$ the normalized values of the PP are, in units of the gap maximum, Δ_0 , $|\Delta_{\uparrow+}| = 0.963$, $|\Delta_{\uparrow-}| = 0.250$, $|\Delta_{\downarrow+}| = 0.822$, $|\Delta_{\downarrow-}| = 0.083$. These numbers can also be approximately inferred from the spin resolved results given by the solid lines in panel (b).

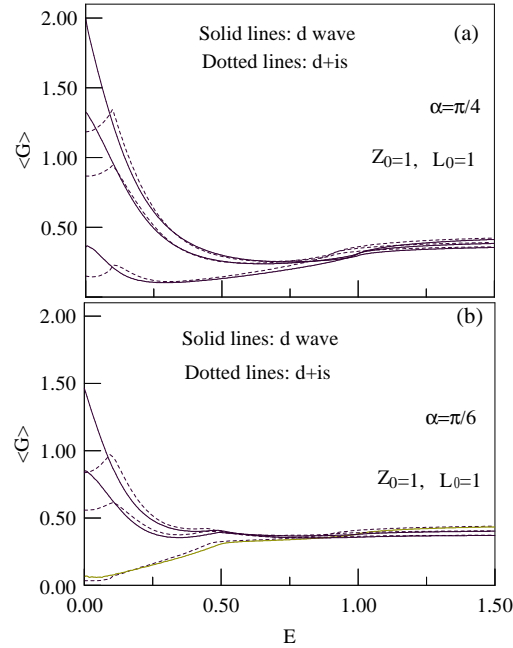


FIG. 8. $\langle G(E) \rangle$, at $Z_0 = 1$, and $L_0 = 1$ for $d_{x^2-y^2}$, and $d_{x^2-y^2} + is$ pair potentials. The latter is of the form $\Delta_{S\pm} = \Delta_0 \cos(2\theta'_{S\pm}) + i0.1\Delta_0$. In panel (a) $\alpha = \pi/4$ and in (b) $\alpha = \pi/6$. From top to bottom (at $E = 0$), the curves correspond to $X = 0, 0.5, 0.9$, in both panels and for each pair potential.

We next turn to the case where there is a nonvanishing potential barrier, choosing for illustration the value $Z_0 = 1$. In the absence of spin polarization, the formation of a ZBCP at finite barrier strength has been extensively investigated^{6,7,10} and explained by Andreev bound states in the context of d -wave superconductivity. We will consider here also the effects of X , not included in previous work. In Fig. 7 we show results for various values of X at $\alpha = \pi/4$. (in panel (a)) and $\alpha = \pi/6$ (panel (b)). One can see that for intermediate values of X the conductance maximum is at finite bias. Comparing the two panels, one sees that the AZB at a fixed $X \neq 0$ is larger for $\alpha = \pi/4$, in agreement with the results obtained for the unpolarized case where, at zero bias, the spectral weight is maximal⁶ for a (110) interface. For a different choice of incident angle θ there will be, if the values of all other parameters are held fixed, a change in the effective barrier strength for various scattering processes. We recall (see below Eq. (2.10)), that $Z = Z_0/\cos\theta$, and with an increase in $|\theta|$ typically there will be, as in the unpolarized case,⁵⁴ a decrease in the amplitude for Andreev reflection and an increased amplitude for ordinary reflection.

Results such as those discussed above can be obtained as a function of angle, and the angular average can then be computed from Eq. (2.12). We will combine showing some of these angularly averaged results with a brief study of another point: it is straightforward to use the formalism discussed here to examine more complicated superconducting order parameters. A question that has given rise to a considerable amount of discussion is that of whether the superconducting order parameter in high T_c materials is pure d -wave or contains a mixture of s wave as well, with an imaginary component, so that there would not be, strictly speaking, gap nodes, but only very deep minima. With this in mind, the effect of a possible “imaginary” PP admixture (for example in a $d + is$ form) on Andreev bound states has also been recently studied.^{13–15} We consider this question here, including the effects of polarization. In Fig. 8, we illustrate the difference in the angularly averaged conductance values obtained for a pure $d_{x^2-y^2}$ PP and

for a mixed $d_{x^2-y^2} + is$ case. We choose the particular form $\Delta_{S\pm} = 0.9\Delta_0 \cos(2\theta'_{S\pm}) + i0.1\Delta_0$. The phase of the PP, $\phi_{S\pm}$, is no longer equal to π or 0 as in the pure d -wave case. We give AA results for several values of X , both for the pure d and the mixed $d + is$ cases.

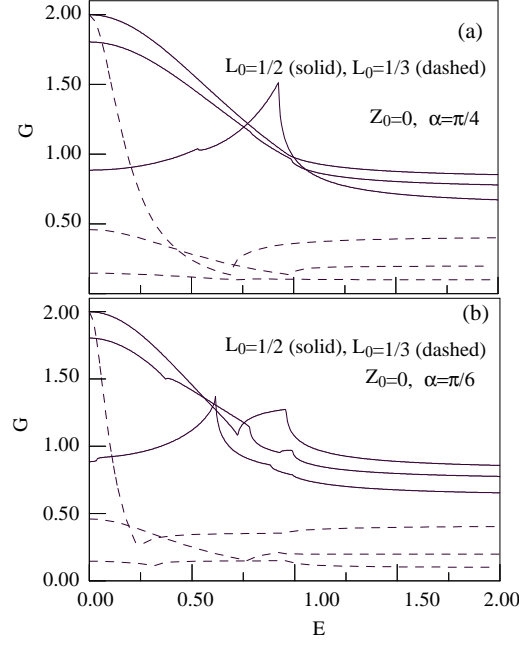


FIG. 9. $G(E)$ for $\theta = \pi/10$, $Z_0 = 0$, and $L_0 = 1/2, L_0 = 1/3$. In panel (a) $\alpha = \pi/4$ and in (b) $\alpha = \pi/6$. From top to bottom, at $E = 0$, curves correspond to $X = 0, 0.5, 0.8$, in both panels and for each pairing potential.

The former represents the angular average of results similar to those previously displayed.

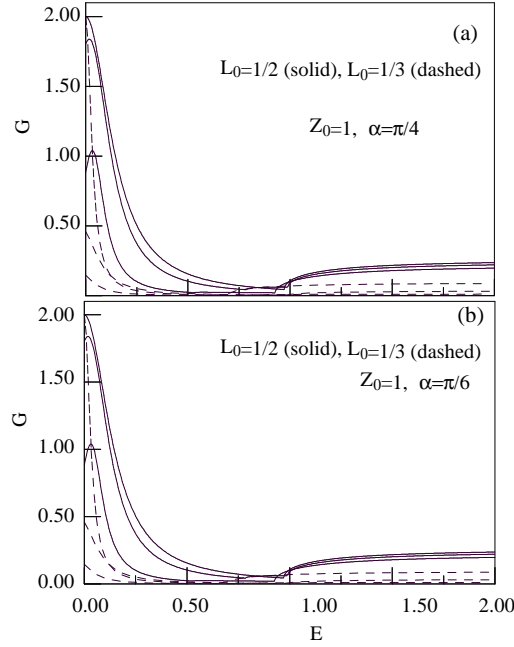


FIG. 10. Conductance curves for $\theta = \pi/10$ at $Z_0 = 1$ with the same parameters and ordering as in Fig. 9.

As in the unpolarized case,^{14,29} the is admixture in the PP is responsible for a FBCP, approximately at $E = 0.1$. The conductance maximum is reduced with increased X and with departure from a (110) oriented interface. Replacing

the $d_{x^2-y^2} + is$ PP by a “real” admixture $d_{x^2-y^2} + s$ (taking again $0.1\Delta_0$ for the s -wave part) gives results almost indistinguishable from the pure d -wave for any value of spin polarization.

To show the effects of FWM on conductance for a pure d -wave PP we take $L_0 = 1/2, 1/3$ and give results at the fixed angle, $\theta = \pi/10$, previously considered. In Fig. 9 we show curves at $Z_0 = 0$ and $\alpha = \pi/4$ (panel (a)), and for $\alpha = \pi/6$ in panel (b). It is useful to compare this figure to panel (a) in Figs. 5, and 6, corresponding to no FWM for $\alpha = \pi/4$ and $\pi/6$, respectively. In the absence of spin polarization the effect of FWM resembles the influence of a nonvanishing barrier strength, Z_0 , and leads to the formation of a ZBCP, which becomes increasingly narrow for smaller L_0 . The effect of moderate spin polarization ($X \lesssim 0.5$, for comparison with the above mentioned figures) on the AZB is rather small for $L_0 = 1, 1/2$ but it is significantly larger at $L_0 = 1/3$. In the next figure, Fig. 10, we use $Z_0 = 1$ and the same parameters as in the previous figure, so that the influence of barrier strength can be gauged. One sees that in the presence of spin polarization the position of the conductance maximum depends on FWM. With increasing mismatch, the FBCP evolves into a ZBCP. By comparing the curves corresponding to $L_0 = 1$ in Fig. 7 with those for smaller L_0 in Fig. 10, it is interesting to notice that an effect similar to that discussed previously for s -wave PP without an interfacial barrier and at normal incidence is also manifested in other regimes, in that the conductance maximum can actually be enhanced, in the spin polarized case (at fixed X), by the FWM.

IV. CONCLUSIONS

In this paper we have studied the conductance spectra of ferromagnetic/superconductor structures. The expressions for Andreev reflection and ordinary reflection amplitudes which we have given, allow one to simply obtain other quantities of interest such as current-voltage characteristics or conductance spectra for spin current.³¹ We have developed the appropriate extensions of the standard approach and approximations used in the absence of spin polarization. This has enabled us to present analytic results. Within these approximations, and with the inclusion of FWM, we have shown a number of important qualitative differences from the unpolarized case or from that where spin polarization is included in the absence of FWM.

Our considerations may also be important in the interpretation of recent experiments^{19,20} attempting to use tunneling to measure the degree of spin polarization in the ferromagnetic side of the junction, since the experimental determination of spin polarization in a ferromagnet is a very difficult and important experimental question in its own right. As we have shown, the ZBCP is sensitive to both spin polarization and FWM, while the gap edge amplitude depends only on X . It is then not possible to straightforwardly determine the spin polarization by using the results for the amplitude of the zero bias conductance unless the appropriate FWM of the F/S structure is known and properly taken into account. Furthermore, FWM can not, unlike in the unpolarized case,³⁷ be simply described by a rescaled value of the interfacial barrier strength.

The procedures used here have the advantages of simplicity and of allowing for analytic solutions. These advantages have enabled us to investigate widely the relevant parameter space. We have left for future work considerations that would have diminished these advantages. Among these are the question of the self consistent treatment of the PP, inclusion of spin-flip scattering or of a more realistic band structure, and non-equilibrium transport. However, we believe that the methods we have employed are sufficient to elucidate the hitherto unappreciated subtleties and the richness and variety of the phenomena associated with spin polarized tunneling spectroscopy.

We hope that our work, as reported here and in Ref. 30, will prompt additional experiments and theoretical work. In particular, an important clue about spin polarized transport would be provided by measurements of the spin resolved conductance. Indeed, we have already become aware of two very recent related preprints leading into these directions, one⁵⁵ on Andreev reflection and spin injection into s - and d -wave superconductors, and another⁵⁶ discussing, in conventional superconductors, out of equilibrium enhanced Andreev reflection with spin polarization.

V. ACKNOWLEDGEMENTS

We would like to thank J. Fabian, A.M. Goldman, A.J. Millis, S. Das Sarma, T. Venkatesan, V.A. Vas’ko, and S. Gasirowicz for useful discussions. This work was supported by the US-ONR.

* Electronic address: igor@cooperon.umd.edu

[†] Electronic address: otvalls@tc.umn.edu

- ¹ J.F. Annett, N. Goldenfeld, and A.J. Leggett, *Physical properties of High Temperature Superconductors V*, D.M. Ginsberg (Ed.), (World Scientific, Singapore, 1996).
- ² D.J. Scalapino, Phys. Repts. **250**, 331 (1995).
- ³ D.J. Van Harlingen, Rev. Mod. Phys. **67**, 515 (1995).
- ⁴ J.A. Sauls, Adv. Phys. **43**, 113 (1994).
- ⁵ Y. Maeno *et al*, Nature **372**, 532 (1994).
- ⁶ C.R. Hu, Phys. Rev. Lett. **72**, 1526 (1994); J. Yang, and C.R. Hu, Phys. Rev. B **50**, 16 766 (1994).
- ⁷ S. Kashiwaya *et al*, Phys. Rev. B **53**, 2667 (1996); Y. Tanaka *et al*, Phys. Rev. Lett. **74**, 3451 (1995).
- ⁸ M. Yamashiro *et al*, Phys. Rev. B **56**, 7847 (1997).
- ⁹ C. Honerkamp and M. Sigrist J. Low Temp. Phys. **111**, 895 (1998).
- ¹⁰ J.W. Ekin *et al*, Phys. Rev. B **56**, 13746 (1997).
- ¹¹ J.Y.T. Wei *et al*, Phys. Rev. Lett. **81**, 2542 (1998).
- ¹² L. Alff *et al*, Phys. Rev. B **58**, 11197 (1998). [Sov. Phys. JETP **19**, 1228 (1964)].
- ¹³ M. Covington *et al*, Phys. Rev. Lett. **79**, 277 (1997).
- ¹⁴ M. Fogelström *et al*, Phys. Rev. Lett. **79**, 281, (1997).
- ¹⁵ J.-X. Zhu and C.S. Ting, Phys. Rev. B **57**, 3038 (1998).
- ¹⁶ M. Matsumoto and H. Shiba, J. Phys. Soc. Jpn. **64**, 3384 (1995).
- ¹⁷ M. Sigrist *et al*, Phys. Rev. B **53**, 2835 (1996).
- ¹⁸ G. Prinz, Phys. Today **48**, 58 (1995).
- ¹⁹ R.J. Soulen *et al*, Science **282**, 85 (1998).
- ²⁰ S.K. Upadhyay *et al*, Phys. Rev. Lett. **81**, 3247 (1998).
- ²¹ M. Johnson, Appl. Phys. Lett. **65**, 1460 (1994).
- ²² V.A. Vas'ko *et al*, Phys. Rev. Lett. **78**, 1134 (1997).
- ²³ Z.W. Dong *et al*, Appl. Phys. Lett. **71**, 1718 (1997).
- ²⁴ V.A. Vas'ko *et al*, Appl. Phys. Lett. **73**, 844 (1998).
- ²⁵ Z. Y. Chen *et al*, unpublished.
- ²⁶ P.M. Tedrow and R. Meservey, Phys. Rev. Lett. **26**, 192 (1971).
- ²⁷ R. Meservey and P.M. Tedrow, Phys. Rep. **238**, 173 (1994).
- ²⁸ M.J.M. de Jong and C.W.J. Beenakker, Phys. Rev. Lett. **74**, 1657 (1995).
- ²⁹ A preprint by J.-X. Zhu *et al* considers some particular cases of F/S junctions without FWM, assuming complete spin polarization, independent of \hbar_0 .
- ³⁰ I. Žutić and O.T. Valls, cond-mat/9808285.
- ³¹ S. Kashiwaya *et al*, cond-mat/9812160, use an approach similar to that in Ref. 30 to calculate the spin current.
- ³² M. Leadbeader *et al*, cond-mat/9811117; R. Seviour *et al*, cond-mat/9811216.
- ³³ A.F. Andreev, Zh. Eksp. Teor. Fiz. **46**, 1823 (1964).
- ³⁴ C. Bruder, Phys. Rev. B **41**, 4017 (1990).
- ³⁵ E. Scheer *et al*, Nature **394**, 154 (1998).
- ³⁶ G.E. Blonder, M. Tinkham and T.M. Klapwijk, Phys. Rev. B **25**, 4515 (1982).
- ³⁷ G.E. Blonder and M. Tinkham, Phys. Rev. B **27**, 112 (1983).
- ³⁸ N.A. Mortensen, K. Flensberg and A.P. Jauho, cond-mat/9807049.
- ³⁹ P.G. de Gennes, *Superconductivity of Metals and Alloys*, (Addison-Wesley, Reading MA, 1989).
- ⁴⁰ M.J. DeWeert and G.B. Arnold Phys. Rev. Lett. **55**, 1522 (1985), M.J. DeWeert and G.B. Arnold Phys. Rev. B **39**, 11307 (1989).
- ⁴¹ Y. Nagato *et al*, J. Low. Temp. Phys. **93**, 33 (1993), give a numerical study of a self-consistent PP for unpolarized s-wave superconductor with FWM.
- ⁴² A. Millis, D. Rainer and J.A. Sauls Phys. Rev. B **38**, 4504 (1988).
- ⁴³ R. Kummel, Phys. Rev. B **16**, 1979 (1977).
- ⁴⁴ A.M. Goldman, private communication.
- ⁴⁵ T. Venkatesan, private communication.
- ⁴⁶ These angles, for various scattering processes, are spin dependent and imply the vanishing of the x component of the appropriate wavevector, as used in Ref. 30.
- ⁴⁷ J.D. Jackson, Classical Electrodynamics (Wiley, New York, 1975), Chapter 7.
- ⁴⁸ S. Kashiwaya *et al*, Phys. Rev. B **51**, 1350 (1995).
- ⁴⁹ This is different from the case of total reflection where there is also no contribution to the conductance above the energy gap.
- ⁵⁰ In Ref. 14, this is modeled by an acceptance cone of angle $2\phi_c$ about the normal and with a uniform weight function $1/2\phi_c$, where ϕ_c is barrier dependent.
- ⁵¹ V.A. Va'sko, private communication.
- ⁵² V.Z. Kresin, G. Deutcher and S.A. Wolf, J. Superconductivity **1**, 327 (1998), V.Z. Kresin and S.A. Wolf, Phys. Rev. B **41**,

4278 (1990).

⁵³ D.R. Harshman and A.P. Millis, Jr., Phys. Rev. B **45**, 10684 (1992).

⁵⁴ S. Chaudhuri and P.F. Bagwell, Phys. Rev. B **51**, 16936 (1995).

⁵⁵ R.L. Merill and Q. Si, cond-mat/9901004.

⁵⁶ O. Bourgeois *et al*, cond-mat/9901045.